arXiv:1612.05520v1 [cond-mat.str-el] 16 Dec 2016

Origin of doping-induced suppression and reemergence of magnetism in $LaFeAsO_{1-x}H_x$

Chang-Youn Moon*

Materials Genome Center, Korea Research Institute of Standards and Science, Yuseong, Daejeon 305-340, Republic of Korea

Hyowon Park

Department of Physics, University of Illinois at Chicago, Chicago, Illinois 60607, USA and Materials Science Division, Argonne National Laboratory, Argonne, Illinois 60439, USA

Kristjan Haule

Department of Physics, Rutgers University, Piscataway, New Jersey 08854, USA

Ji Hoon Shim†

Department of Chemistry, Pohang University of Science and Technology, Pohang 790-784, Republic of Korea

(Dated: December 19, 2016)

Abstract

We investigate the evolution of magnetic properties as a function of hydrogen doping in iron based superconductor $LaFeAsO_{1-x}H_x$ using the dynamical mean-field theory combined with the density-functional theory. We find that two independent consequences of the doping, the increase of the electron occupation and the structural modification, have the opposite effects on the strength of electron correlation and magnetism, resulting in the minimum of the calculated magnetic moment around the intermediate doping level as a function of x. Our result provides a natural explanation for the puzzling recent experimental discovery of the two separated antiferromagnetic phases at low and high doping limits. Furthermore, the increase of orbital occupation and correlation strength with the doping results in reduced orbital polarization of $d_{xz/yz}$ orbitals and the enhanced role of d_{xy} orbital in the magnetism at high doping levels, and their possible implications to the superconductivity are discussed in line with the essential role of the magnetism.

PACS numbers: 71.15.Mb, 71.27.+a, 74.20.Pq, 74.70.Xa

Keywords:

I. INTRODUCTION

Iron-based high temperature (T) superconductors including the seminal material $LaFeAsO_{1-x}F_x$[1] share a common feature that the impurity doping results in the suppression of magnetic and/or structural orders in undoped parent compounds and subsequent emergence of superconductivity. The underlying mechanism is still not well understood, however, as the impurity doping has several independent effects on the system such as the change of the electron occupancy, structural modification, and occurrence of the disorder, etc. One of the popular explanations has been based on the itinerant picture of the antiferromagnetic (AFM) ordering in undoped samples. As the doping changes the number of carriers and the position of the Fermi level, the Fermi surface (FS) nesting condition for the spin density wave (SDW) formation becomes poorer.[2–5] However, the non-negligible role of the electron correlation in these materials has been pointed out,[6–8] and the validity of the FS nesting picture alone, which assumes the rigid band against the carrier doping, often turns out to be doubtful in explaining the emergence and suppression of the AFM order. On the other hand, the structural modification effect is known to alter significantly the magnetic property with the strong magnetostructural coupling in this system.[2,9,10] Even the isovalent impurity doping or the hydrostatic pressure alone, which introduce no extra carrier, can give rise to the similar phase diagram with the case of the carrier doping.[11–15]

There is a general consensus about the importance of the magnetism in understanding the superconductivity of iron-based materials,[16,17] as the magnetism is omnipresent in this class of materials at least in the form of the short-range spin fluctuation.[18–20] However, the basic nature of the magnetism has been controversial among the SDW of itinerant electrons,[2–5,21] the Heisenberg type interactions of localized spins,[22–25] as well as their intermediate picture.[26–35] Nevertheless, the spin fluctuation has been widely accepted as the most probable candidate for the pairing glue for the superconductivity.[36–42] In the meanwhile, there are also growing arguments and evidences for the presence of the orbital order and fluctuations in these materials.[43–54] Recent experiments on FeSe suggest that the orbital degree of freedom drives the electronic nematicity and spontaneous symmetry breaking instead of the spin degree of freedom,[55,56] drawing attention for the alternative mechanism of the pairing mediated by the orbital fluctuation.[57,58] Because the spin and orbital degrees of freedom are coupled each other,[43,59] however, there can be an inherent ambiguity in

determining which order forms first and drives the other.

Recently, a series of experiments has revived the attention to the seminal material of the family by the hydrogen (H) doping, namely, $LaFeAsO_{1-x}H_x$.[60–62] Overcoming the solubility limit of the conventional fluorine dopant, hydrogen can increase the doping concentration up to $x = 0.6$. Surprisingly, another superconducting and AFM phases adjacent to each other are found at high doping levels, analogously to their conventional counterparts at the low doping level (see Fig. 1(a)). Posing fundamental questions on the nature of magnetism and superconductivity, this finding is expected to give a clue for still unresolved issues mentioned earlier. Although some theoretical attempts have been made to explain the appearance of the second AFM phase mostly focusing on the FS nesting property in the itinerant electron picture,[60,61,63] first-principles approach simultaneously incorporating the itinerant and localized aspects of the system is desirable when we consider the 'moderately correlated' nature of these materials[6–8,64,65] and some unsatisfactory conclusions from the itinerant picture such as the prediction of an incorrect magnetic ordering vector.[61]

In this paper, we investigate the magnetic and electronic properties of $LaFeAsO_{1-x}H_x$ as a function of x using the combined method of density-functional theory plus dynamical mean-field theory (DFT+DMFT), which captures the material-specific electronic correlation.[66,67] Considering changes of both electron occupancy and lattice structure caused by the hydrogen doping which turn out to have the opposite effects on the electron correlation and magnetism, we find that both static magnetic moment and local magnetic susceptibility initially decrease to the minimum at around $x = 0.3$ and then increase again up to $x = 0.6$, in agreement with the experimental phase diagram of the two separate AFM phases centered at $x = 0$ and 0.5. More electron occupation at $d_{xz/yz}$ orbitals with the doping enhances the importance of the d_{xy} orbital in the static magnetic moment and also in spin dynamics, while reducing the orbital polarization. Our results emphasize the importance of the electron correlation and structural modification in understanding the doping induced evolution of the electronic structure, and also the magnetism as an indispensable ingredient for the emergence of the superconductivity in these materials.

II. CALCULATION METHOD

We use the modern implementation of DFT+DMFT method within all electron embedded DMFT approach,[67] where in addition to correlated Fe atoms the itinerant states of other species are included in the Dyson self-consistent equation. The strong correlations on the Fe ion are treated by DMFT, adding self-energy $\Sigma(\omega)$ on a quasi atomic orbital in real space, to ensure stationarity of the DFT+DMFT approach. The self-energy $\Sigma(\omega)$ contains all Feynman diagrams local to the Fe ion. No downfolding or other approximations were used, and the calculations are all-electron as implemented in Ref. 67, which is based on Wien2k.[68] We used the GGA exchange-correlation functional,[69] and the quantum impurity model was solved by the continuous time quantum Monte Carlo impurity solver[70] using $U = 5.0$ eV and $J = 0.72$ eV. Brillouin zone integration is done on the 12×12×6 k-point mesh for the AFM unitcell of LaFeAsO containing 4 Fe atoms. All calculations are done for $T = 150$ K. We consider both paramagnetic (PM) and AFM states at this temperature. The AFM state is considered to represent the actual stable phase observed in experiments, while the PM state is also calculated to understand the driving force with which the AFM state is stabilized from a 'bare' state.

III. RESULTS

A. Electronic correlation and magnetic strengths as functions of doping

Schematic phase diagram of $LaFeAsO_{1-x}H_x$ in the $x-T$ space is depicted in Fig. 1(a). The first AFM phase with a stripe-type order is rapidly suppressed and disappears around $x = 0.05$ with the emergence of the first superconducting phase followed by the adjacent second superconducting phase. Further doping initiates the second AFM phase, of the same ordering pattern with the first AFM phase, but with a slightly different atomic displacement.[62] We perform the DFT+DMFT calculations to check if this suppression and reappearance of the AFM phase can be reproduced. To take the electron doping effect into account, we adopt the virtual crystal approximation.[60] In addition, the structural change due to the H doping is incorporated by interpolating both the lattice constants and internal atomic coordinates of the available experimental values at $x = 0$[71] and $x = 0.51$[62] in the PM states with the tetragonal lattice symmetry. This should be a reasonable approximation considering the

almost linear As height dependence on x observed experimentally,[60] avoiding the difficulty in the structural optimization of alloy structures within DFT which would require rather complicated statistical treatment, besides concerns about the general reliability of DFT in predicting the accurate lattice structure of iron-based superconducting materials. Using this doping scheme, the static magnetic moment and the local spin susceptibility, $\chi_{local}(\omega = 0) = \int_0^\beta \langle S(\tau)S(0)\rangle \mathrm{d}\tau$, are calculated as a function of x for the stripe-type AFM phase and shown in Fig. 1(b). The magnetic moment at $x = 0$ is estimated to be 0.66 μ_B with an agreement with the measured value 0.63 μ_B,[72] and decreases to the minimum value of 0.12 μ_B at $x = 0.4$, and then exhibits a rapid increase to reach 0.68 μ_B at $x = 0.6$. The local susceptibility shows a similar behavior with a minimum at $x = 0.3$, implying that the overall magnetic strength is suppressed and then re-enhanced with the doping. Therefore, we verify that the DFT+DMFT method captures the essential underlying physics of two separate AFM phases in this material and produces a consistent behavior of the local magnetic strength, while the complete suppression of magnetic phase and emergence of the superconducting phase in the intermediate x as shown in Fig. 1(a) could not be properly described within the current calculation scheme. For comparison, we perform the DFT calculation on the relative stability of the AFM phase and the magnetic moment as functions of x. For $x = 0$, the AFM phase is found to be 180 meV/Fe more stable than the nonmagnetic phase with the magnetic moment of 2.15 μ_B. Upon increasing x, the stability of AFM phase and the magnetic moment show no discernible change, suggesting that the normal DFT calculation cannot properly describe the observed evolution of the magnetism.

Then we investigate the underlying mechanism of the doping-induced change of the electronic structure by considering the electron addition and structural modification separately. Because the nominal number of valence electrons in a Fe atom for the undoped material is six, which corresponds to an electron doped system from the half-filled orbitals, further electron doping should result in the monotonic decrease of the correlation strength.[73] On the other hand, the H doping increases the distance between Fe and surrounding As atoms as determined experimentally,[62,71] which would lead to the localization of Fe d orbitals.[74] To confirm this speculation, we estimate the mass enhancement $1/Z = 1 - \frac{\partial \Sigma(\omega)}{\partial \omega}|_{\omega=0}$ for the two effects separately. First, we calculate $1/Z$ of the d_{xy} in the PM phase as a function of x considering only the electron addition effect by fixing the lattice structure to that of $x = 0$ as in Fig. 1(c). Indeed, $1/Z$ monotonically increases with the electron addition. On the con-

trary, when only the structural effect is included without extra electron, $1/Z$ monotonically decreases with increasing x. When these two competing effects are combined, $1/Z$ increases overall with the doping, which means that the localization by the structural modification becomes more dominant at the highly doped system.

This competing effects are also reflected on the magnetic strength of the AFM phase as shown in Fig. 1(d). When only electron addition effect is considered, the local susceptibility is found to monotonically decrease with increasing x, while it increases monotonically when only the structural modification is taken into account (with the number of extra electrons fixed to 0.6), in agreement with the behavior of the mass enhancement factors in Fig. 1(c). Therefore, we can conclude that the initial suppression and the later re-enhancement of the magnetism with the H doping originates from the two competing effects : the electron addition and increasing Fe-As distance which suppresses and enhances the local correlation and hence the local magnetism, respectively. Our analysis naturally draws attention to the important role of the electron correlation and also the structural effect in understanding the doping induced phase diagram of this material. Suppression of the magnetism and the existence of the quantum criticality in phosphorus-doped Ba122 systems $BaFe_2As_{2-x}P_x$[75–77] are another set of examples which demonstrate the dramatic effect of the pure structure modification, where decreased Fe-anion distance was pointed out to cause the suppression of the magnetism.[76]

B. Fermi surfaces

We also investigate the evolution of the FS with the doping which is generally considered to be relevant to the existence of the AFM phase.[61,63] The FSs for three different doping levels, x =0, 0.3, and 0.5, are calculated with both the DFT+DMFT and DFT methods and displayed in Fig. 2. Starting with a relatively good nesting between the hole and electrons surfaces at $x = 0$ for the DFT case, the doping degrades the nesting with shrinking the hole surfaces at the Γ point and enlarging the electron surfaces at the M point (see Fig. 2(g)-(i)), as the electron doping raises the Fermi level. Our result shows a good agreement with the previous DFT calculation using the experimentally determined lattice structure,[60] confirming that our assumption of the linear dependence of the lattice constants and internal atomic coordinates is reasonable. The DFT+DMFT results shown in Figs. 2(a)-(f) are qualitatively

similar, but the d_{xy} hole FS expands compared with the DFT results, because of more correlated nature of the d_{xy} orbital than $d_{xz/yz}$ orbitals as pointed out in the DFT+DMFT study of LiFeAs.[78] The decrease of the overall spectral weight with the doping and relatively larger incoherence of the d_{xy} surface reflect the larger correlation at high doping levels and for the d_{xy} orbital (Figs. 2(a)-(c)). Nevertheless, both levels of the theory indicate the monotonic degradation of the FS nesting with the doping, as already indicated by previous calculations,[60,63] manifesting that the FS nesting alone cannot explain the appearance of the second AFM phase. Again, we conclude that the electron correlation and many-body effects should be incorporated to understand the doping-induced evolution of the magnetism.

C. Spin resolved spectral function

To understand the doping-induced suppression and the reemergence of the magnetism in detail, we investigate the spin-resolved spectral function of the d_{xy} orbital in the AFM phase as a function of x as shown in Fig. 3. At $x = 0$, the majority and minority spin states exhibit a large exchange splitting reflecting the overall magnetic moment of 0.66 μ_B, with a distinct pseudo-gap feature (a dip in spectral function) at the Fermi energy induced by the coupling between the electron and hole bands at the Fermi energy.[31] With increasing doping level up to $x = 0.3$ (see Fig. 3(a)), spectral weights moves from the peak just above the Fermi level to one below the Fermi energy in the minority spin channel, suggesting the doped electrons fills the minority spin states. The electron filling in the minority spin states with the doping naturally leads to the gradual reduction of the exchange splitting and the magnetic moment, along with the size of the pseudo-gap. On the other hand, further doping over $x = 0.3$ enhances the exchange splitting as shown in Fig. 3(b), which seems to almost retrace the evolution of the spectral function from $x = 0$ to $x = 0.3$ in Fig. 3(a). However, there are several noticeable differences as well. First, the pseudo-gap position is constantly shifting deeper in the valence states with its size and the magnetic moment increasing with increasing x, which indicates the rise of the Fermi energy as a result of the electron doping. More importantly, doping over $x = 0.3$ develops a shoulder growing with x near -1 eV in the majority spin channel as indicated by a arrow in Fig. 3(b), contributing to build up the magnetic moment against the electron filling on the minority spin states with the doping. The spectral weight piled up in this position results from many-body

effects and hence is incoherent, rather than from the shift of coherent quasi-particle states. The inset of Fig. 3(b) depicts the imaginary part of the d_{xy} component of the electron self energy (ImΣ) along with the spectral function for $x = 0.6$. One can identify a strong peak of the ImΣ around -0.7 eV, close to the J value 0.72 eV adopted in this study, and the shoulder structure of the spectral function at a nearby position, suggesting that the shoulder structure originates from the incoherent excitations related to the self energy. Similar energy scales between this incoherent excitation and J is also consistent with the suggestion that iron-based superconductors are Hund's metals where J plays more important role than U.[7]

D. Orbital polarization

As mentioned earlier, the orbital order is of great interest for these materials regarding the electronic nematicity and also superconductivity itself. Here we compare the orbital polarization, i.e., the imbalance between $d_{xz/yz}$ orbitals, in the AFM state for low and high doping cases. For $x = 0$ as displayed in Fig. 4(a), d_{xz} and d_{yz} spectral functions show noticeable difference, where the spin polarization is larger for d_{yz} as well as d_{xy} orbitals while d_{xz} spin splitting is smaller. On the other hand, for the high doping case of $x = 0.5$ in Fig. 4(b), $d_{xz/yz}$ components of the spectral function becomes much more similar with each other and now the d_{xy} orbital has the most significant spin polarization. Indeed, our estimated orbital polarization $(n_{xz} - n_{yz})/(n_{xz} + n_{yz})$ decreases from 3.9 % at $x = 0$ to 1.5 % at $x = 0.5$ while the magnetic moments for the two cases are comparable. Increasing x enhances the crystal field splitting pushing up the d_{xy} level above $d_{xz/yz}$ level, so that the doped electrons fill $d_{xz/yz}$ orbitals first rather than the d_{xy} orbital, reducing the imbalance between $d_{xz/yz}$ orbitals as well as between their spin components. Meanwhile, besides the less electron filling, the elevated As height in the high doping case further enhances the electron correlation for the d_{xy} orbital via the 'kinetic frustration'[79] compared with the $d_{xz/yz}$ orbitals. So d_{xy} becomes the most significant component for the local spin fluctuations in the PM phase and for static magnetic moments in the AFM phase. Therefore, at high doping levels, strong local magnetism appears mainly from d_{xy} orbital and the orbital polarization from $d_{xz/yz}$ is largely suppressed.

E. Spin excitation spectrum

So far, we have considered the doping induced evolution of the magnetically ordered state, and we will conclude our discussion by investigating the dynamic spin fluctuations in the PM state, which is more relevant to the superconductivity, as a function of the doping. Although $T = 150$ K at which the calculation is done is close to the AFM transition temperature, the spin susceptibility in the PM state is expected to be a smooth varying function of T (except at the AFM ordering wave vector for which the susceptibility diverges at the AFM transition temperature), so we expect qualitatively similar results for other temperatures. We evaluate the dynamical spin structure factor $S(\mathbf{q},\omega) = \frac{\chi''(\mathbf{q},\omega)}{1-e^{\hbar\omega/k_BT}}$ using the DFT+DMFT method as displayed in Fig. 5, where both the one-particle Green's function and the local two-particle vertex function are determined *ab-initio*.[80] For $x = 0$, the spin excitation spectrum has strong peaks near the zero energy around the wave vector $\mathbf{q} = (\pi, 0)$, which corresponds to the magnetic ordering vector of the AFM phase, and disperses over the path shown in the spectrum, reaching a maximum energy at the zone boundary $\mathbf{q} = (\pi, \pi)$, all consistent with previous results.[41,80,81] As the doping level x increases, the overall spin excitation spectral weights tend to shift to lower energies as the spin wave dispersion decreases with the increasing correlation strength. The excitation near $\mathbf{q} = (\pi/2, \pi/2)$ noticeably goes down towards the zero energy with the doping, and a new possible static magnetic order for this wave vector is suggested for $x = 0.5$. However, the intensity of excitations has always the maximum at the conventional AFM ordering vector $\mathbf{q} = (\pi, 0)$ for all the doping cases, consistent with the experimentally found second AFM phase for the high doping levels.[62] For $S(\mathbf{q},\omega)$ at $\mathbf{q} = (\pi + \delta, 0)$ which is slightly off the magnetic ordering vector, as shown in Fig. 5(d), the peak height near the zero energy is reduced for $x = 0.3$ compared with that for $x = 0$ indicating the suppressed tendency towards the static magnetic order, and then it becomes pronounced again for the higher doping level $x = 0.5$ suggesting the re-enhanced magnetism, which shows a qualitative agreement with the initial decrease and re-enhancement of the calculated magnetic moment in the AFM phase shown in Fig. 1 and again also with the motivating experiments.[61,62] When decomposed by orbitals (see Figs. 5(e)-(g)), the $d_{xz/yz}$ components show a large anisotropy with the d_{yz} component peak being dominant at $x = 0$. As the doping level increases, the $d_{xz/yz}$ anisotropy keeps decreasing while the d_{xy} component becomes most prominent. The

decreasing $d_{xz/yz}$ anisotropy and the enhancement of the d_{xy} component with the increasing doping is consistent with the features observed in our result for the AFM phase.

IV. DISCUSSION

Our results remind us of the indispensable role of the electron correlation in the iron-based superconducting materials, as well as the impact of the structural change. The doping-induced evolution of the electronic and magnetic properties cannot be understood by simply adopting the rigid shift of the Fermi level or even the self-consistent addition of carriers without taking the structural effect into account. In addition, a natural view on the doping-induced evolution of spin and orbital orders can be obtained. The 'ferro-orbital order', which is coupled to the AFM spin order in the undoped materials, is the lowest-energy configuration for the nominally half-filled orbitals to maximize the kinetic energy gain.[43] Both the orbital and spin orders of d_{xz} or d_{yz} are suppressed when the doping supplies more electrons to these orbitals away from the half-filling. The d_{xy} orbital, for which the spin order can form but the orbital order is no longer relevant, becomes the dominant channel for the electron hopping to reduce the kinetic energy as discussed above. As a result, spin order/fluctuation is present near the both superconducting domes found in $LaFeAsO_{1-x}H_x$ while orbital order/fluctuation is expected to be strong only near the first superconducting phase in the lower doping level. Our results consequently suggests that the spin fluctuation is more closely related to the superconductivity, at least for the second superconducting phase in this alloy, while the orbital fluctuation, which is significant only at low doping levels, might not be a prerequisite for the superconductivity in general. The enhanced role of the d_{xy} orbital in magnetism is expected to naturally lead to its dominant role also in the superconductivity with a larger FS hole pocket of this orbital as shown in Fig. 2. Although the enhanced electron correlation and consequent stronger spin fluctuation in the higher doping level might contribute to the strong superconductivity, too strong correlation would be harmful to the superconductivity, out of several reasons,[79] due to the lowered magnon energy scale (Fig. 5) which is directly coupled to the size of the superconducting gap. Further theoretical study which directly attacks the superconductivity as a function of the doping level will be desirable.

V. CONCLUSION

In summary, by adopting the DFT+DMFT method, where the local dynamic correlation effect is taken exactly, we successfully reproduce the hydrogen-doping-induced suppression and revitalization of the magnetism in $LaFeAsO_{1-x}H_x$ which has been recently established experimentally. Taking the structural modification by the doping into account along with the carrier addition is found to be essential, as the two factors induce independent and opposite effects on the electron correlation strength and the magnetism in this alloy. Doping reduces the orbital imbalance between $d_{xz/yz}$ orbitals as well as their magnetic activity, while the d_{xy} orbital becomes the dominant electron hopping channel with increased electron correlation and the magnetic strength for high doping levels. Indispensable role of the electron correlation and detailed atomic structure is identified in understanding the electronic and magnetic properties, and the magnetism possibly as more fundamental ingredient in realizing the superconductivity is suggested over the orbital degrees of freedom.

Acknowledgments

This research was supported by Basic Science Research Program through the National Research Foundation of Korea (NRF) funded by the Ministry of Science, ICT and Future Planning (2016R1C1B1014715 and 2015R1D1A1A01059621).

---

* Electronic address: cymoon@kriss.re.kr

† Electronic address: jhshim@postech.ac.kr

[1] Y. Kamihara, H. Hiramatsu, M. Hirano, R. Kawamura, H. Yanagi, T. Kamiya, and H. Hosono, J. Am. Chem. Soc. **128**, 10012, (2006); Y. Kamihara, T. Watanabe, M. Hirano, and H. Hosono, J. Am. Chem. Soc. **130**, 3296, (2008).

[2] D. J. Singh and M.-H. Du, Phys. Rev. Lett. **100**, 237003 (2008).

[3] I. I. Mazin, M. D. Johannes, L. Boeri, K. Koepernik, and D. J. Singh, Phys. Rev. B **78**, 085104 (2008).

[4] V. Cvetkovic and Z. Tesanovic, Europhys. Lett. **85**, 37002 (2009).

[5] J. Dong *et al.*, Europhys. Lett. **83**, 27006 (2008).

[6] K. Haule, J. H. Shim, and G. Kotliar, Phys. Rev. Lett. **100**, 226402 (2008).

[7] K. Haule and G. Kotliar, New J. Phys. **11**, 025021 (2009).

[8] M. Yi, D. H. Lu, R. Yu, S. C. Riggs, J.-H. Chu, B. Lv, Z. K. Liu, M. Lu, Y.-T. Cui, M. Hashimoto, S.-K. Mo, Z. Hussain, C. W. Chu, I. R. Fisher, Q. Si, and Z.-X. Shen, Phys. Rev. Lett. **110**, 067003 (2013).

[9] Z. P. Yin, S. Lebegue, M. J. Han, B. P. Neal, S. Y. Savrasov, and W. E. Pickett, Phys. Rev. Lett. **101**, 047001 (2008).

[10] T. Yildirim, Phys. Rev. Lett. **102**, 037003 (2009).

[11] Z. A. Ren, G. C. Che, X. L. Dong, J. Yang, W. Lu, W. Yi, X. L., Shen, Z. C. Li, L. L. Sun, F. Zhou, and Z. X. Zhao, Europhys. Lett. **83**, 17002 (2008).

[12] C. Wang, S. Jiang, Q. Tao, Z. Ren, Y. Li, L. Li, C. Feng, J. Dai, G. Cao, and Z. Xu, Europhys. Lett. **86**, 47002 (2009).

[13] T. Park, E. Park, H. Lee, T. Klimczuk, E. D. Bauer, F. Ronning, and J. D. Thompson, J. Phys.: Condens. Matter **20**, 322204 (2008).

[14] H. Okada, K. Igawa, H. Takahashi, Y. Kamihara, M. Hirano, H. Hosono, K. Matsubayashi, and Y. Uwatoko, J. Phys. Soc. Jpn. **77**, 113712 (2008).

[15] H. Mukuda, F. Engetsu, T. Shiota, K. T. Lai, M. Yashima, Y. Kitaoka, S. Miyasaka, and S. Tajima, J. Phys. Soc. Jpn. **83**, 083702 (2014).

[16] P. J. Hirschfeld, M. M. Korshunov, and I. I. Mazin, Rep. Prog. Phys. **74**, 124508 (2011).

[17] C. H. Lee, P. Steffens, N. Qureshi, M. Nakajima, K. Kihou, A. Iyo, H. Eisaki, and M. Braden, Phys. Rev. Lett. **111**, 167002 (2013).

[18] S. Li, C. de la Cruz, Q. Huang, Y. Chen, J. W. Lynn, J. Hu, Y.-L. Huang, F.-C Hsu, K.-W. Yeh, M.-K. Wu, and P. Dai, Phys. Rev. B **79**, 054503 (2009).

[19] S. Iikubo, M. Fujita, S. Niitaka, and H. Takagi, J. Phys. Soc. Japan **78**, 103704 (2009).

[20] Y Qiu, W Bao, Y. Zhao, C. Broholm, V. Stanev, Z. Tesanovic, Y. C. Gasparovic, S. Chang, J. Hu, B. Qian, M. Fang, and Z. Mao, Phys. Rev. Lett. **103**, 067008 (2009).

[21] R. S. Dhaka, S. E. Hahn, E. Razzoli, R. Jiang, M. Shi, B. N. Harmon, A. Thaler, S. L. Bud'ko, P. C. Canfield, and A. Kaminski, Phys. Rev. Lett. **110**, 067002 (2013).

[22] Q. Si and E. Abrahams, Phys. Rev. Lett. **101**, 076401 (2008).

[23] L. X. Yang, Y. Zhang, H. W.Ou, J. F. Zhao, D. W. Shen, B. Zhou, J. Wei, F. Chen, M. Xu, C. He, Y. Chen, Z. D. Wang, X. F. Wang, T. Wu, G. Wu, X. H. Chen, M. Arita, K. Shimada, M.

Taniguchi, Z. Y. Lu, T. Xiang, D. L. Feng, Phys. Rev. Lett. **102**, 107002 (2009).

[24] T. Yildirim, Phys. Rev. Lett. **101**, 057010 (2008).

[25] J. Zhao, Y. Shen, R. J. Birgeneau, M. Gao, Z.-.Y. Lu, D.-H. Lee, X. Z. Lu, H. J. Xiang, D. L. Abernathy, and Y. Zhao, Phys. Rev. Lett. **112**, 177002 (2014).

[26] J. Wu, P. W. Phillips, and A. H. Castro Neto, Phys. Rev. Lett. **101**, 126401 (2008).

[27] J. Wu and P. W. Phillips, J. Phys.: Condens. Matter **23**, 094203 (2011).

[28] S.-P. Kou, T. Li, and Z.-Y. Weng, Europhys. Lett. **88**, 17010 (2009).

[29] G. D. Samolyuk and V. P. Antropov, Phys. Rev. B **79**, 052505 (2009).

[30] J. Zhao, D. T. Adroja, D.-X. Yao, R. Bewley, S. Li, X. F. Wang, G. Wu, X. H. Chen, J. Hu, and P. Dai, Nat. Phys. **5**, 555 (2009).

[31] C.-Y. Moon, S. Y. Park, and H. J. Choi, Phys. Rev. B **80**, 054522 (2009).

[32] C.-Y. Moon and H. J. Choi, Phys. Rev. Lett. **104**, 057003 (2010).

[33] H. Ikeda, R. Arita, and J. Kunes, Phys. Rev. B **81**, 054502 (2010).

[34] Z. P. Yin, K. Haule, and G. Kotliar, Nat. Phys. **7**, 294 (2011).

[35] P. Dai, J. Hu, and E. Dagotto, Nat. Phys. **8** 709, (2012).

[36] I. I. Mazin, D. J. Singh, M. D. Johannes, and M. H. Du, Phys. Rev. Lett. **101**, 057003 (2008).

[37] J. Zhang, R. Sknepnek, R. M. Fernandes, and J. Schmalian, Phys. Rev. B **79**, 220502(R) (2009).

[38] C. H. Lee, K. Kihou, H. Kawano-Furukawa, T. Saito, A. Iyo, H. Eisaki, H. Fukazawa, Y. Kohori, K. Suzuki, H. Usui, K. Kuroki, and K. Yamada, Phys. Rev. Lett. **106**, 067003 (2011).

[39] G. F. Ji, J. S. Zhang, L. Ma, P. Fan, P. S. Wang, J. Dai, G. T. Tan, Y. Song, C. L. Zhang, P. Dai, B. Normand, and W. Yu, Phys. Rev. Lett. **111**, 107004 (2013).

[40] Y. M. Dai, B. Xu, B. Shen, H. Xiao, H. H. Wen, X. G. Qiu, C. C. Homes, and R. P. S. M. Lobo, Phys. Rev. Lett. **111**, 117001 (2013).

[41] Z. P. Yin, K. Haule, and G. Kotliar, Nat. Phys. **10**, 845 (2014).

[42] M. P. Allan, K. Lee, A. W. Rost, M. H. Fischer, F. Massee, K. Kihou, C.-H. Lee, A. Iyo, H. Eisaki, T.-M. Chuang, J. C. Davis, and E.-A. Kim, Nat. Phys. **11**, 177 (2015).

[43] C.-C. Lee, W.-G. Yin, and W. Ku, Phys. Rev. Lett. **103**, 267001 (2009).

[44] W. Lv, F. Kruger, and P. W. Phillips, Phys. Rev. B **82**, 045125(2010).

[45] C.-C. Chen, J. Maciejko, A. P. Sorini, B. Moritz, R. R. P. Singh, and T. P. Devereaux, Phys. Rev. B **82**, 100504(R) (2010).

[46] W.-C. Lee, W. Lv, J. M. Tranquada, and P. W. Phillips, Phys. Rev. B **86**, 094516 (2012).

[47] W.-C. Lee and P. W. Phillips, Phys. Rev. B **86**, 245113 (2012).

[48] V. Stanev and P. B. Littlewood, Phys. Rev. B **87**, 161122(R) (2013).

[49] Y. K. Kim, W. S. Jung, G. R. Han, K.-Y. Choi, C.-C. Chen, T. P. Devereaux, A. Chainani, J. Miyawaki, Y. Takata, Y. Tanaka, M. Oura, S. Shin, A. P. Singh, H. G. Lee, J.-Y. Kim, and C. Kim, Phys. Rev. Lett. **111**, 217001 (2013).

[50] C. Ma, L. Wu, W.-G. Yin, H. Yang, H. Shi, Z. Wang, J. Li, C. C. Homes, and Y. Zhu, Phys. Rev. Lett. **112**, 077001 (2014).

[51] S. Liang, A. Mukherjee, N. D. Patel, C. B. Bishop, E. Dagotto, and A. Moreo, Phys. Rev. B **90**, 184507 (2014).

[52] H. Kontani and Y. Yamakawa, Phys. Rev. Lett. **113**, 047001 (2014).

[53] T. Saito, Y. Yamakawa, S. Onari, and H. Kontani, Phys. Rev. B **92**, 134522 (2015).

[54] S. Mukherjee, A. Kreisel, P. J. Hirschfeld, and B. M. Andersen, Phys. Rev. Lett. **115**, 026402 (2015).

[55] S.-H. Baek, D. V. Efremov, J. M. Ok, J. S. Kim, J. van den Brink, and B. Buchner, Nat. Mater. **14**, 210 (2015).

[56] A. E. Bohmer, T. Arai, F. Hardy, T. Hattori, T. Iye, T. Wolf, H. v. Lohneysen, K. Ishida, and C. Meingast, Phys. Rev. Lett. **114**, 027001 (2015).

[57] H. Kontani and S. Onari, Phys. Rev Lett. **104**, 157001 (2010).

[58] Y. Yanagi, Y. Yamakawa, and Y. Ono, Phys. Rev. B **81**, 054518 (2010).

[59] R. M. Fernandes, A. V. Chubukov, and J. Schmalian, Nat. Phys. **10**, 97 (2014).

[60] S. Iimura, S. Matsuishi, H. Sato, T. Hanna, Y. Muraba, S. W. Kim, J. E. Kim, M. Takata, and H. Hosono, Nat. Comm. **3**, 943 (2012).

[61] N. Fujiwara, S. Tsutsumi, S. Iimura, S. Matsuishi, H. Hosono, Y. Yamakawa, and H. Kontani, Phys. Rev. Lett. **111**, 097002 (2013).

[62] M. Hiraishi, S. Iimura, K. M. Kojima, J. Yamaura, H. Hiraka, K. Ikeda, P. Miao, Y. Ishikawa, S. Torii, M. Miyazaki, I. Yamauchi, A. Koda, K. Ishii, M. Yoshida, J. Mizuki, R. Kadono, R. Kumai, T. Kamiyama, T. Otomo, Y. Murakami, S. Matsuishi, and H. Hosono, Nat. Phys. **10**, 300 (2014).

[63] K. Suzuki, H. Usui, S. Iimura, Y. Sato, S. Matsuishi, H. Hosono, and K. Kuroki, Phys. Rev. Lett. **113**, 027002 (2014).

[64] D. H. Lu, M. Yi, S.-K. Mo, A. S. Erickson, J. Analytis, J.-H. Chu, D. J. Singh, Z. Hussain, T.

H. Geballe, I. R. Fisher, and Z.-X. Shen, Nature (London) **455**, 81 (2008).

[65] M. M. Qazilbash, J. J. Hamlin, R. E. Baumbach, Lijun Zhang, D. J. Singh, M. B. Maple, and D. N. Basov, Nat. Phys. **5**, 647 (2009).

[66] G. Kotliar, S. Y. Savrasov, K. Haule, V. S. Oudovenko, O. Parcollet, and C. A. Marianetti, Rev. Mod. Phys. **78**, 865 (2006).

[67] K. Haule, C.-H Yee, and K. Kim, Phys. Rev. B **81**, 195107 (2010).

[68] P. Blaha, K. Schwarz, G. Madsen, D. Kvasnicka and J. Luitz, *WIEN2k* (Vienna University of Technology, Vienna, Austria, 2001).

[69] J. P. Perdew, K. Burke, and M. Ernzerhof, Phys. Rev. Lett. **77**, 3865 (1996).

[70] K. Haule, Phys. Rev. B **75**, 155113 (2007).

[71] K. Nomura, S. W. Kim, Y. Kamihara, M. Hirano, P. V. Sushko, K. Kato, M. Takata, A. L. Shluger, and H. Hosono, Supercond. Sic. Technol. **21**, 125028 (2008).

[72] N. Qureshi, Y. Drees, J. Werner, S. Wurmehl, C. Hess, R. Klingeler, B. Buchner, M. T. Fernandez-Diaz, and M. Braden, Phys. Rev. B **82**, 184521 (2010).

[73] L. de' Medici, G. Giovannetti, and M. Capone, Phys. Rev. Lett. **112**, 177001 (2014).

[74] H doping reduces the lattice constants which seems to be natural considering the smaller size of H than O species which is replaced. Meanwhile, the Fe-As distance turns out to increase with the doping, which might be understood by imagining that the reduced thickness of LaO layers by H doping decompresses adjacent FeAs layers allowing the Fe-As distance to increase.

[75] S. Jiang, H. Xing, G. Xuan, C. Wang, Z. Ren, C. Feng, J. Dai Z. Xu, and G. Cao, J. Phys.:Condens. Matter **21**, 382203 (2009).

[76] M. Rotter, C. Hieke, and D. Johrendt, Phys. Rev. B **82**, 014513 (2010).

[77] J. G. Analytis, H.-H. Kuo, R. D. McDonald, M. Wartenbe, P. M. C. Rourke, N. E. Hussey, and I. R. Fisher, Nat. Phys. **10**, 194 (2014).

[78] G. Lee, H. S. Ji, Y. Kim, C. Kim, K. Haule, G. Kotliar, B. Lee, S. Khim, K. H. Kim, K. S. Kim, K.-S. Kim, and J. H. Shim, Phys. Rev. Lett. **109**, 177001 (2012).

[79] Z. P. Yin, K. Haule, and G. Kotliar, Nat. Mater. **10**, 932 (2011).

[80] H. Park, K. Haule, and G. Kotliar, Phys. Rev. Lett. **107**, 137007 (2011).

[81] C. Zhang, L. W. Harriger, Z. P. Yin, W. Lv, M. Wang, G. Tan, Y. Song, D. L. Abernathy, W. Tian, T. Egami, K. Haule, G. Kotliar, and P. Dai, Phys. Rev. Lett. **112**, 217202 (2014).

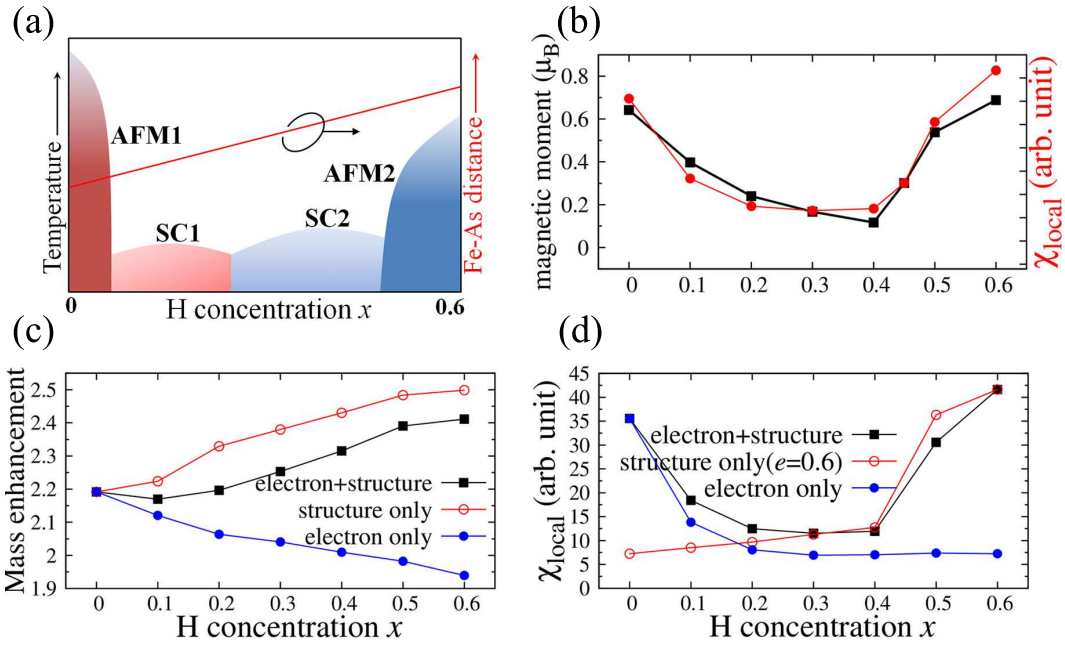

FIG. 1: (color online) (a) Schematic phase diagram of $LaFeAsO_{1-x}H_x$ for the the hydrogen concentration x and temperature. AFM1 and AFM2 denote the first and second AFM phases, while SC1 and SC2 represent the first and second superconducting phases, respectively. Note that the bond length between Fe and As atoms increases with x. (b) Local magnetic moment and magnetic susceptibility $\chi_{local}(\omega = 0)$ in the AFM phase as a function of x, which exhibit minimums around $x = 0.3$. (c) Mass enhancement $1/Z$ is calculated as a function of x with three different treatments of the doping in the PM phase: both electron addition and structural change are included (filled squares), only structural change is allowed while no extra electron is added (empty circles), and extra electron is added with x while fixing the structure to that of $x = 0$ case (filled circles). (d) Local magnetic susceptibility as a function of x in the AFM phase for three different treatments for doping analogously to (c). For the structure only case, we use the number of extra electrons fixed to that for the $x = 0.6$ case.

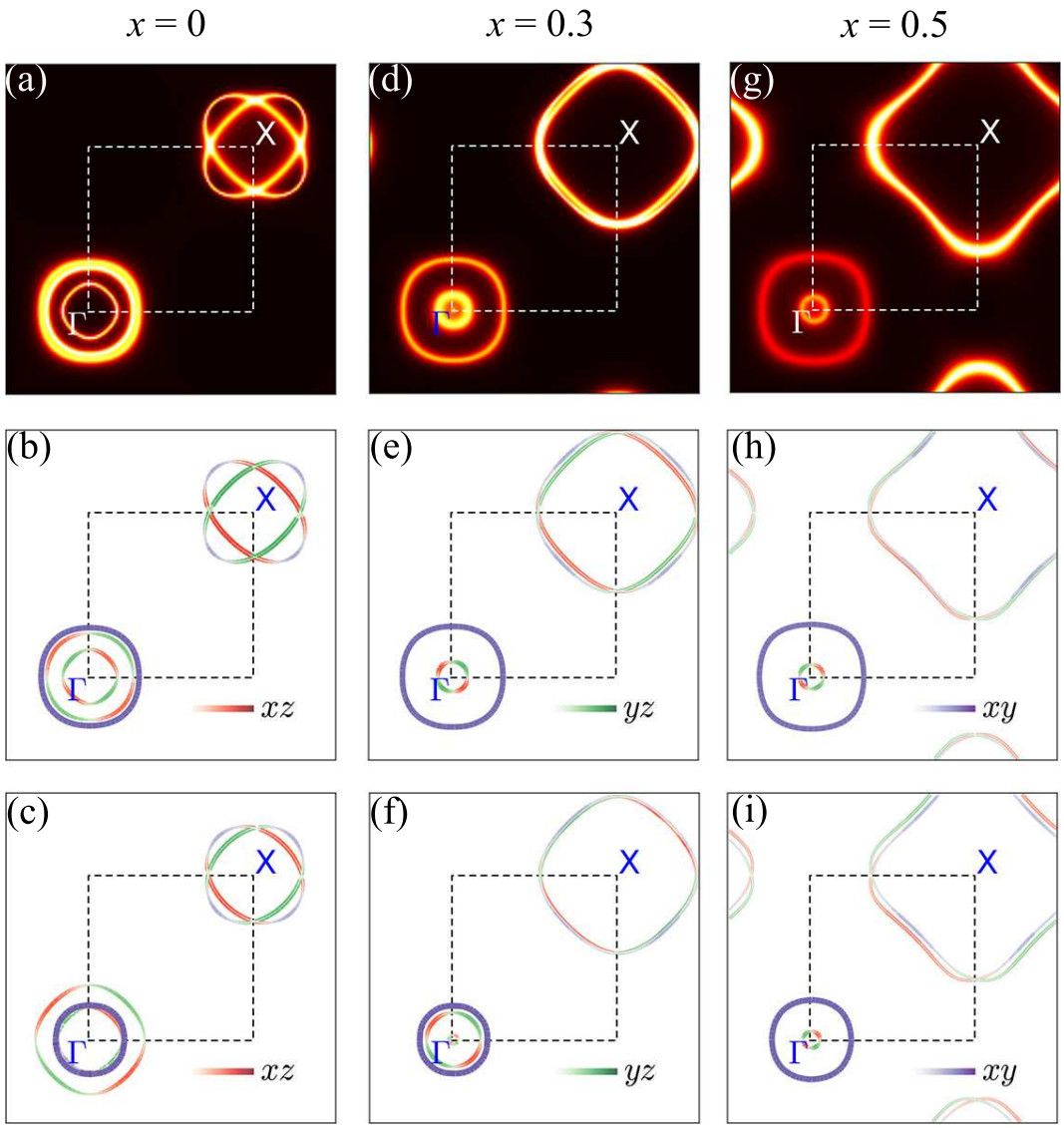

FIG. 2: (color online) FS for (a)-(c) $x = 0$, (d)-(f) $= 0.3$, and (g)-(i) $x = 0.5$ calculated on the $k_z = 0$ plane of the PM phase. Top rows are plots of A(k,$\omega = 0$) from the DFT+DMFT calculations, and middle rows denote their Fe d orbital characters, while bottom rows are from the usual DFT calculations. Each orbital character is represented by the depth of the assigned color as well as the thickness of the Fermi surface line.

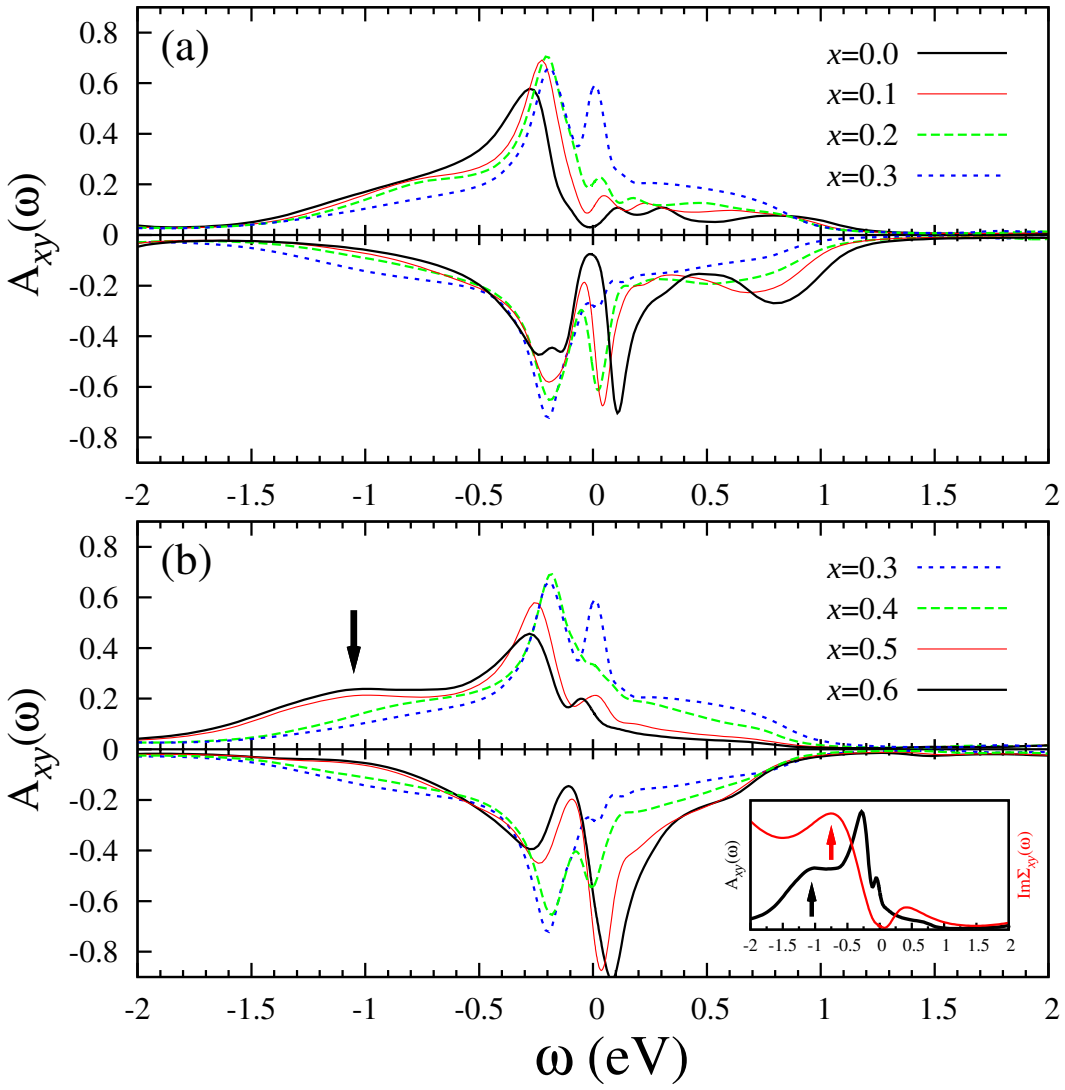

FIG. 3: (color online) The spectral function projected onto the Fe d_{xy} orbital of an Fe atom, $A_{xy}(\omega)$, with majority and minority spin channels displayed in positive and negative axes, respectively, in the AFM phase. (a) From $x = 0$ to $x = 0.3$, the magnetic moment decreases with decreasing exchange splitting. (b) From $x = 0.4$ to $x = 0.6$, the magnetic moment increases. Inset depicts $A_{xy}(\omega)$ in the black line for majority spin channel of $x = 0.6$. The shoulder structure around -1 eV indicated by a black arrow is correlated with the peak structure in $\mathrm{Im}\Sigma_{xy}(\omega)$ in the red line at a slightly higher energy location as indicated by a red arrow.

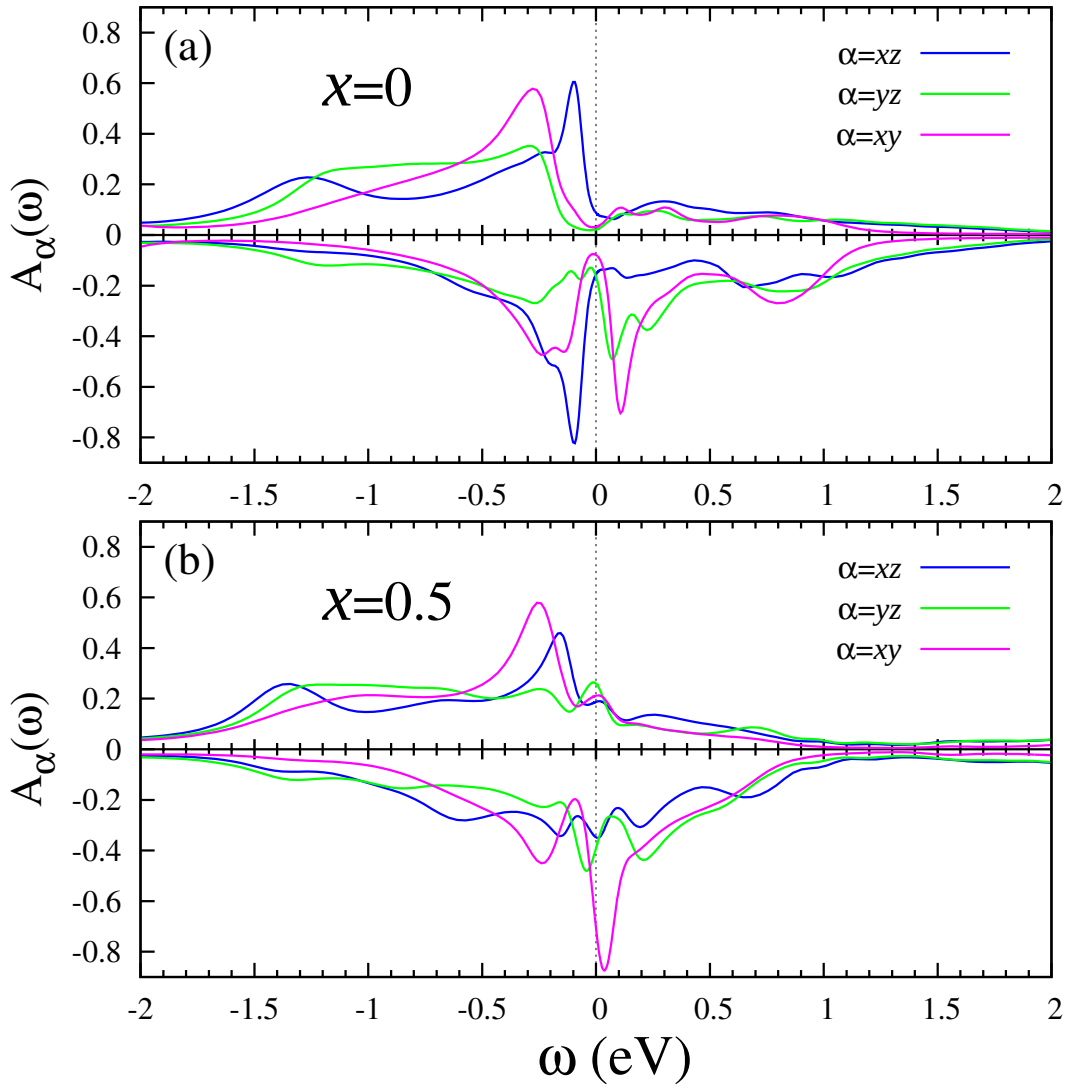

FIG. 4: (color online) The spectral function in the two spin channels in the AFM phase, projected onto d_{xz}, d_{yz}, and d_{xy} orbitals in a Fe atom, for (a) $x = 0$ and (b) $x = 0.5$. The orbital order which corresponds to the difference between xz and yz components is suppressed at $x = 0.5$ compared with $x = 0$.

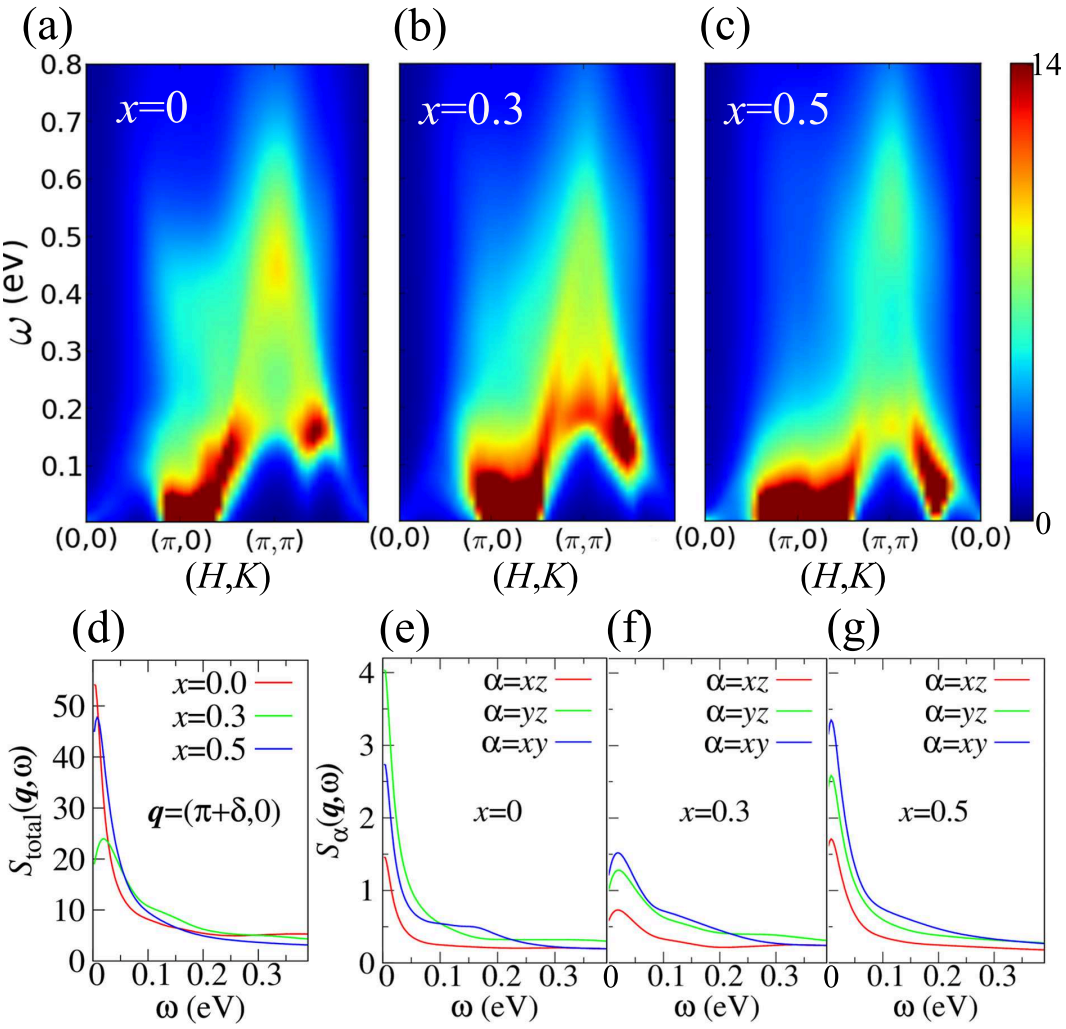

FIG. 5: (color online) Dynamic spin structure factor $S(\mathbf{q},\omega)$ in the PM state for (a) $x = 0$, (b) $x = 0.3$, and (c) $x = 0.5$ is plotted along the high-symmetry path $(H, K, L = \pi)$ in the first Brillouin zone of the single-iron unit cell, where $(H, K) = (\pi, 0)$ is the AFM ordering vector. (d) Total $S(\mathbf{q},\omega)$ is plotted as a function of ω for different x at the fixed momentum $q = (\pi+\delta, 0)$, which is slightly off the AFM ordering vector at which the spin susceptibility diverges below the AFM transition temperature. Here we take $\delta = -0.0625\pi$. Orbital decomposed $S(\mathbf{q},\omega)$ is displayed also at $q = (\pi + \delta, 0)$ for (e) $x = 0$, (f) $x = 0.3$, and (g) $x = 0.5$.